City Research Online

City, University of London Institutional Repository

Citation: Malgarinos, I., Nikolopoulos, N. & Gavaises, M. (2017). Numerical investigation of heavy fuel droplet-particle collisions in the injection zone of a Fluid Catalytic Cracking reactor, Part I: Numerical model and 2D simulations. Fuel Processing Technology, 156, pp. 317-330. doi: 10.1016/j.fuproc.2016.09.014

This is the accepted version of the paper.

This version of the publication may differ from the final published version.

Permanent repository link: https://openaccess.city.ac.uk/id/eprint/17238/

Link to published version: https://doi.org/10.1016/j.fuproc.2016.09.014

Copyright: City Research Online aims to make research outputs of City, University of London available to a wider audience. Copyright and Moral Rights remain with the author(s) and/or copyright holders. URLs from City Research Online may be freely distributed and linked to.

Reuse: Copies of full items can be used for personal research or study, educational, or not-for-profit purposes without prior permission or charge. Provided that the authors, title and full bibliographic details are credited, a hyperlink and/or URL is given for the original metadata page and the content is not changed in any way.

City Research Online: http://openaccess.city.ac.uk/ publications@city.ac.uk

Numerical investigation of heavy fuel droplet-particle collisions in the injection zone of a Fluid Catalytic Cracking reactor, Part I: Numerical model and 2D simulations

Ilias Malgarinos[1*], Nikolaos Nikolopoulos[1,2] and Manolis Gavaises[1]
1: School of Mathematics, Computer Science & Engineering, City University London, Northampton Square, EC1V 0HB London, UK, *Corresp. Author – e-mail: Ilias.Malgarinos.1@city.ac.uk
2: Centre for Research and Technology Hellas, Chemical Process and Energy Resources Institute, Egialeias 52, Marousi, Athens, Gr-15125, Greece

Abstract

The present paper investigates the collisions between heavy gasoil droplets and solid catalytic particles taking place at conditions realized in Fluid Catalytic Cracking reactors (FCC). The computational model utilizes the Navier-Stokes equations along with the energy conservation and transport of species equations. The VOF methodology is used in order to track the liquid-gas interface, while a dynamic local grid refinement technique is adopted, so that high accuracy is achieved with a relative low computational cost. Phase-change phenomena (evaporation of the heavy gasoil droplet), as well as catalytic cracking surface reactions are taken into account. Physical properties of heavy and light molecular weight hydrocarbons are modeled by representative single component species, while a 2-lump scheme is proposed for the catalytic cracking reactions. The numerical model is firstly validated for the case of a single liquid droplet evaporation inside a hot gaseous medium and impingement onto a flat wall for droplet heating and film boiling conditions. Afterwards, it is utilized for the prediction of single droplet-catalyst collisions inside the FCC injection zone. The numerical results indicate that droplets of similar size to the catalytic particles tend to be levitated more easily by hot catalysts, thus resulting in higher cracking reaction rates/cracking product yield, and limited possibility for liquid pore blocking. For larger sized droplets, the corresponding results indicate that the production of cracking products is not favored, while solid-liquid contact increases. Hotter catalysts promote catalytic cracking reactions and droplet levitation over the catalytic particle, owed to the formation of a thin vapour layer between the liquid and the solid particle.

Keywords: VOF; FCC; droplet; particle; collisions; cracking

Nomenclature

Acronyms		S	Source (dependent on equation)
CFD	Computational Fluid Dynamics	SSA	Specific Surface Area (m^2/g)
cpR	Cells per Radius	T	Time (s)
DTP	Droplet To Particle size ratio	T	Temperature (K)
FCC	Fluid Catalytic Cracking	$\vec{u}$ (u,v,w)	Velocity (its components) (m/s)
LBM	Lattice-Boltzmann method	V	Volume (m^3)
LPG	Liquefied petroleum gas	$We=\rho_{liq}u_0^2D_0/\sigma$	Weber number (-)
MW	Molecular weight (kg/kmol)	X	Mole fraction (mole-specie/mole-gas)
UDF	User defined Function	Y	Mass fraction (kg-specie/kg-gas)
VOF	Volume of Fluid Method		
Symbols		Greek letters	
$[X]$	Kmol-Xspecie/m^3-gas	A	Liquid volume fraction (-)
A	Pre-exponential factor	β_m	thermal accommodation coefficient
A_{int}	Interface Surface Area (m^2)	H	Direction normal to wall
D	Droplet Diameter (m)	Θ	contact angle (^{o})
D_{diff}	Diffusivity (m^2/s)	M	dynamic viscosity (kg/ms)
E	Energy (J/kg) ($h-p/\rho+u^2/2$)	ρ	Density (kg/m^3)
E_a	Activation Energy (consistent units with R_u)	σ	surface tension coefficient (N/m)
h	Enthalpy (J/kg)	T	Non-dimensional time ($=tu_o/D_o$)
J	Diffusion flux (kg/m^2s)		
k	Kinetic constant ($m^6/(kmol \cdot kg_{cat} \cdot s)$	*Subscripts*	
k_{cond}	Effective conductivity (W/mK)	∞	Far from the interface (outside the Knudsen layer)
Kn	Knudsen number	b	Boiling
L	Latent Heat (J/kg)	e	Energy
m	Mass (kg)	g	Gas
$\dot{m}, \dot{m}'$	Vaporization rate (kg/m^2s, kg/m^3s)	l	liquid
p	Pressure (Pa)	o	initial condition
$Re=\rho_l u_0 D_0/\mu_l$	Reynolds number (-)	p	particle
RR	Reaction rate ($kmol/g_{cat}s$)	sat	Saturated
R_u	Universal Gas Constant (=8314.47 J/kmolK)	v	vapour

1. Introduction

The collision of a liquid droplet with a solid surface of any shape is a physical phenomenon that appears in many technological applications, such as for example, spray cooling, spray coating and fuel injection in internal combustion engines. Another very interesting application of droplet dynamics is found in the Fluid Catalytic Cracking (FCC) industry and concern droplet-particle collisions. FCC units, which are integral parts of modern fossil fuel refineries, are used to convert heavy fuel, named as “gas oil” coming from the distillation unit, to lighter products like gasoline or LPG. The conversion is achieved via the “cracking” reaction, i.e. the decomposition of high, long carbon chain/high molecular weight hydrocarbons to smaller chain/lower molecular weight products. This reaction is accommodated within the FCC reactor, where hot fluidized solid catalysts come in contact with the atomized heavy oil droplets, and takes place at the surface of the catalysts, which are porous solids, such as zeolites.

In most CFD works published on the FCC rectors, the whole reactor hydrodynamics is simulated without considering the detailed mechanisms taking place at the time and length scales of droplet impact. A common assumption which is made [1-5] is that the feed is quickly vaporized after its spraying into the reactor, due to the high temperature of the solid catalyst (higher than the liquid boiling point). In these studies, a 2-phase flow approach is used in order to simulate the mixing/reactions of solid catalysts with gas flowing inside FCC reactors. In [6, 7] however, the importance of studying the FCC injection zone, and more specifically the liquid feed vaporization is highlighted, as it is an important aspect for the correct calculation of the cracking yields and products selectivity. For this reason, in recent CFD works [6-11] the additional investigation of the injected droplets motion, coupled with a vaporization model has been performed. This has allowed the full 3-phase (solid catalysts/liquid droplets/gas) problem exhibited in real FCC reactors to be resolved, where however the detail achieved in the injection zone is not enough to capture the real interactions occurring between cold injected droplets and hot catalytic particles.

Additionally, the direct contact between liquid drops and porous catalysts that occurs in the FCC injection zone, may lead to the deactivation of the catalysts, from the insertion/blocking of their pores with non-evaporated liquid [12]. This phenomenon, signifies the importance to focus more in this zone and particularly in droplet-particle interactions and specifically investigate the direct solid-liquid contact. Moreover, the life duration of a single droplet is very important, considering that the catalyst to oil mass weight ratio within FCC reactors is in the range of 4:1 up to 10:1 [13]. Interface tracking methods can provide the advanced level of detail needed in order to study these micro-scale phenomena.

In previous efforts to investigate these phenomena, i.e. in numerical/experimental works that focus on droplet dynamics in FCC reactors, only three works were tracked [14-16] in the open literature. Gac and Gradon [14] investigated the outcome of droplet-particle isothermal collisions using the Lattice-Boltzmann method (LBM); in their work, all operating conditions are provided in dimensionless format. Mitra et al. [16] have presented numerical simulations and experiments related to droplet impingement onto a spherical particle under both isothermal and non-isothermal conditions. However, the liquids they used were water, isopropyl alcohol and acetone, the choice of which seems to be far from resembling real gasoil behaviour. Finally, Ge and Fan [15] have presented numerical simulations of non-isothermal droplet collision with a solid particle using the Level-Set (LS) method and the Immersed Boundary Method (IBM) for the representation of the solid phase. In their work, they have coupled their numerical model with a 2D model for the vapour boundary layer, in order to incorporate the effect of the thermal boundary layer formed between the liquid interface and the solid surface, in collisions under film boiling conditions. Overall, the temperature and impact velocity range of values examined in the last two works are significantly lower than the ones exhibited under realistic FCC conditions.

The aim of this study is to investigate, by means of CFD, the collision of a single droplet with catalytic particles, under realistic FCC operating conditions. In this paper (Part I), the numerical background of the CFD model utilized will be presented, followed by the simulation of single droplet-particle collision scenarios on 2D axisymmetric domains. In the following paper (Part II), 3-D simulations are included both for single droplet-particle collisions and for droplet impact on a cluster of particles. To the best of authors' knowledge, no similar study shedding light in the cracking reaction and the pore blocking mechanism exists in the open literature; the results of this study can assist in modifying the injection strategy in FCC reactors towards higher cracking product yield and lower catalyst deactivation rates.

In the following sections, brief literature review on FCC injection zone operating conditions, as well as cracking reaction modelling approaches will be presented.

1.1 Operating conditions in the FCC injection zone

A typical image of the path that a droplet follows in the injection zone of an FCC reactor is depicted in Figure 1a. More information on this subject can be found in the work of Patel et al. [17] where the authors follow a 1-D Lagrangian approach for the interpretation of the spray behaviour.

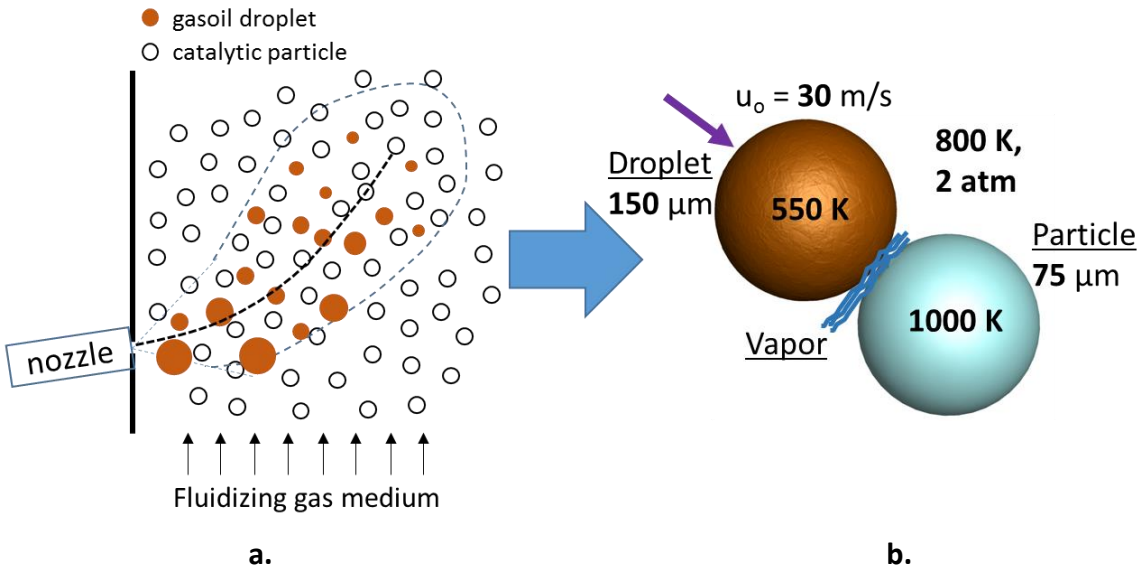

Figure 1. a) Mean path of injected droplets and b) Operating conditions of droplet-particle collisions

The conditions that should be taken into account throughout the droplet path are: *a) injection conditions* such as feed preheat (478-673 K [13, 18]), injected drop velocity (45 to 100m/s [13]) and drop sizes (50-500µm [6, 8, 17]), *b) reactor conditions*, like bed pressure (1.5-3 bar (Table 10.2 of [19])) and temperature (769-838K [13]), as well as *c) catalyst conditions*, such as size (60-75 µm [6, 7, 17]), mean velocity (6-17m/s [13, 17]) and temperature (950-1005K [13]). The mean operating conditions for droplet-particle collisions inside the FCC injection zone were gathered from selective representative studies [1, 3-10, 13, 17-19] and are presented in Figure 1b.

1.2 Cracking path and liquid-gas properties for petroleum fractions (lumping)

In the majority of CFD works related to the FCC reactors [1, 3-10], the hydrodynamic equations are coupled with lump reaction kinetics in order to present a holistic/general view of the reactor/catalytic cracking yields. The “lump” species, as they are called, are groups of different species that exhibit similar behaviour and are used in order to overcome the difficulty that lies in the characterization of the exact components that constitute petroleum fraction liquids and the exact catalytic cracking reactions products. In other words, such type of schemes are assumed to be a good representation of the most influential reactions taking place in such complex systems (a large variety of varying properties species and phases are actual in the real case) and for that reason, the same approach has been decided to be followed in the present study. The first lumping scheme was proposed by Weekman and Nace in 1970 [20], namely the 3-lump kinetic scheme, which grouped the kinetics of an FCC reactor in gasoil, gasoline,

light gases and coke species. Later on, in 1988, Yen et al. [21] split the third lump to separate light gases and coke lumps respectively, and formulated the most commonly used [1, 3, 6, 17, 22] 4-lump scheme. More detailed 9-lump [4] and 12-lump schemes [10] can also be found. However, these models have not been coupled so far with the detailed hydrodynamic and heat transfer taking place during the collisions between liquid droplets and solid particles. As a first step towards the prediction of the influence that micro-scale hydrodynamic conditions may have on the catalytic cracking yields and pore blocking mechanism, a simplified 2-lump scheme is used, which is presented in Figure 2.

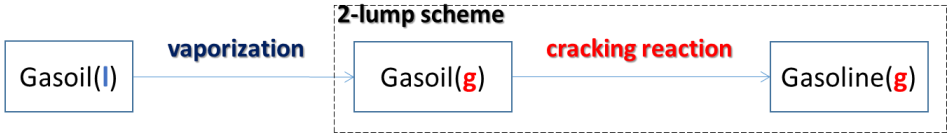

Figure 2. Cracking path used in this work. From gasoil liquid to gasoline gas.

The selection of this 2-lump scheme is justified as the introduction of more gas species into the mixture (LPG, light gases, coke) that are products of cracking reactions) would rise the complexity of the problem; at the same time the use of a coke deactivation function is not needed as coke deposition is a phenomenon lasting in the range of ms [23], which is greater than the droplet impingement itself (0.01ms). In addition to that, deactivation models currently available in the literature do not account for the microscopic level of the direct solid-liquid contact between the droplets and the catalytic particle surface but only depend on residence time [1, 6, 10] and are mainly applicable for larger-scale simulations.

For the gasoil and gasoline lumps, the physical properties varying with temperature of n-pentacosane ($C_{25}H_{52}$) and n-heptane (C_7H_{16}) chemical species have been used as representative of real fluids (Carl L. Yaws properties [24-26]). For petroleum fractions, varying properties are usually calculated based on empirical correlations [27], in contrast to single component hydrocarbons [24]. The criteria for the choice of the single component hydrocarbons were molecular weight and liquid density, based on values gathered from relevant works [1, 3-10] (gasoil - $MW_{literature}$=226-450, $MWC_{25}H_{52}$=352.691, $\rho_{literature}$=610-924.8, ρ_{C25H52}=801.16, gasoline – $MW_{literature}$=100-117.8, MWC_7H_{16}=100.205). The use of single component to represent petroleum fractions has been presented in a thermodynamic evaluation of FCC reactor [28]. The fluidizing medium is considered to be water-vapor (H_2O), commonly used in the FCC industry.

It should be pointed out that the physical properties used [24-26] refer to conditions of 101,325 Pa pressure, while the diffusivity concerns hydrocarbon-air mixtures. It is assumed that these properties do not change significantly for the operating conditions of the cases simulated in this study, refering to a 202,650 Pa operating pressure, where water vapour is the surrounding gas, as can be seen from the empirical work of [29] or similar ones.

2. Numerical Methodology

2.1 Fluid flow and Volume of Fluid Method

The Navier-Stokes equations are utilised for the prediction of fluid flow, while the Volume of Fluid (VOF) Method is used for liquid-gas interface tracking [30, 31]. The numerical equations are solved in the ANSYS/FLUENT software [32], which has been extended with the implementation of a dynamic local grid refinement technique using custom built UFDs and was presented in a previous work of the same authors [33]. Using this technique, the grid is refined close to the liquid-gas interface and follows its motion dynamically, while the computational cost is decreased compared to a uniform grid having the same resolution [33]. The current model, has been validated for droplet impact onto solid flat and spherical surfaces under isothermal conditions [33, 34]; in this work it is extended to account for heat transfer, phase change and surface "cracking" reactions, as will be presented in the following sections.

2.2 Phase change evaporation model

The extension of the VOF model to non-isothermal flows in order to account for the evaporation of the liquid phase is achieved with the additional solution of the energy equation, as well as the transport equation of the produced vapour. These equations are presented here, together with the updated volume fraction equation, accounting for the mass transfer mechanisms (source terms):

$$\frac{\partial \rho E}{\partial t} + \nabla \cdot \left[\vec{u}(\rho E + p) \right] = \nabla \cdot \left(k_{cond} \nabla T - (1-\alpha) \sum_j h_j J_j \right) + S_e \quad (1)$$

$$\frac{\partial (1-\alpha) \rho_g Y_j}{\partial t} + \nabla \cdot \left[(1-\alpha) \rho_g \vec{u} Y_j \right] = \nabla \cdot \left[-(1-\alpha) J_j \right] + S_v \quad (2)$$

$$\frac{1}{\rho_l} \left[\frac{\partial \alpha \rho_l}{\partial t} + \nabla \cdot \left(\vec{u} \alpha \rho_l \right) = S_l \right] \quad (3)$$

Energy E and temperature T are treated as mass-weighted variables. Inter-species diffusion is accounted for by the second term on the right hand side of the energy equation, where J_j is the diffusion flux of species j of the gas mixture:

$$J_j = -\rho_g \, \mathrm{D}_{\mathrm{diff},j} \nabla \mathrm{Y}_j \qquad (4)$$

Source terms are incorporated in volume fraction, vapour transport and energy conservation equations in order to represent the mass transfer of liquid to vapour phase and the latent heat of evaporation during the phase change process, respectively. These source terms are presented in Table 1. The latent heat is replaced by the difference of formation enthalpies of liquid and vapour, as depicted in Table 1.

The mass transfer rate used is based on the kinetic theory of gases [35] and is given by the following equation:

$$\dot{m} = \frac{2\beta_m}{2-\beta_m}\sqrt{\frac{MW}{2\pi R_u}}\left(\frac{\mathrm{P}_{\mathrm{sat}}}{T_{sat}} - \frac{\mathrm{P}_{\infty}}{T_{\infty}}\right) \quad [\mathrm{kg/m^2 s}] \qquad (5)$$

This equation is valid to be used for the operating conditions of this study (weak evaporation for Kn << 1 and $(T_{oo}-T_b)/T_b$ << 1) as stated in [36]. The thermal accommodation coefficient β_m represents the proportion of molecules that hit the liquid surface and are absorbed by it [36]. Its value ranges from 0 to 1, and in this work it takes the value of 0.5 [37], as scarce information can be found on its exact values especially concerning heavy hydrocarbons [36].

For the implementation of eq. 5, in the interface cells, saturation pressure P_{sat} is derived [26] from local cell value T_{sat}, as the interface is supposed to be saturated, while the properties far from the interface, outside the Knudsen layer [36] (denoted with the symbol ∞) are calculated from the neighbour cell whose centre is closer to the direction of the interface unit normal gradient (negative so that it points outwards of the interface). The partial pressure of the vapour phase is calculated by Dalton's Law, given the mass concentration of vapour in the specific cell:

$$p_{\infty} = X_i p_{gas}, \quad X_i = \frac{Y_i / MW_i}{\sum_i Y_i / MW_i}, \qquad (6)$$

where X_i is the mole fraction and Y_i is the mass fraction of each specie in a multicomponent droplet approximation. P_{gas} is the operating pressure (202,650 Pa in this work).

The mass transfer rate, in order to be compliant with the units of the volume fraction and transport of vapor species equations is transformed into:

$$\dot{m}' = \dot{m}\frac{A_{\mathrm{int}}}{V} = \dot{m}\frac{|\nabla\alpha|V}{V} = \dot{m}|\nabla\alpha| \quad [\mathrm{kg/m^3 s}] \qquad (7)$$

where A_{int} is the interfacial surface area of the droplet, and it is equal to the magnitude of the volume fraction gradient multiplied by the computational cell volume [38, 39].

Using this evaporation model, the cells of the interface are not explicitly set as saturated, but this condition is derived from the solution of vapour transport equation (eq. 2).

2.3 Surface Reactions Modelling

The basic principles of catalytic cracking reactions are presented in the textbook of Froment and Bischoff [40] and concern the transport of heavy molecular weight gaseous species from the main stream, to the catalyst surface, then to its pore up to a catalytic site in order to react. In the scope of the present study, the catalytic reaction can only be regarded from a wider perspective, meaning that the particle surface is represented by a spherical geometry discretized by a finite number of faces, i.e. without discretizing the exact porous geometry. This is incorporated implicitly via the variable "SSA" as explained below.

In numerical terms, the additional transport of gasoline lump specie equation is solved (similar to eq. 2), coupled with its production through gasoil cracking (Figure 2). Moreover, the following equation is solved:

$$\rho_{gas} D_i \frac{\partial Y_i}{\partial \eta} = MW_i \frac{RR}{SSA} \quad \text{[kg/m}^2\text{s]} \quad (8)$$

in order to get the unknown value of Y_i at each wall boundary face, which is used as a fixed value boundary condition in the gasoline lump transport equation. The variable SSA is the catalyst particle Specific Surface Area given in m^2 per catalyst weight and is used under the assumption that the wall area at each boundary cell represents the real pore area available for catalytic cracking reactions. Reaction rate kinetics are taken from the work of Gianetto et al. [41], and are presented in Table 1. Reaction rate and kinetic constant k are given by the following expressions [41]:

$$RR = k\left[C_{25}H_{52}\right]^2 \quad \text{[kmol/g}_{cat}\text{s]} \quad (9)$$

$$k = Ae^{(-E_a/R_uT)} \quad (10)$$

Evaporation		Cracking Reaction Parameters	
Equation	Source Term	Variable	Value
Energy	$S_e = -\dot{m}' L = -\dot{m}'(h_v^f - h_l^f)$	A	0.4272e+13 $m^6/(kmol \cdot kg_{cat} \cdot s)$
Vapor	$S_v = \dot{m}'$	E_a	21009.9 cal/mol
Volume fraction	$S_v = -\dot{m}'$	Specific Surface Area (SSA)	269 m^2/g

Table 1. Evaporation source terms incorporated in respective equations and cracking reaction kinetics (pre-exponential factor, activation energy and specific surface area) used for 2-lump scheme taken from [41].

Before advancing to the results section, it should be pointed out that in the framework of this study, many UDFs have been developed to assist the implementation of new models into ANSYS FLUENT software. These UDFs include new material libraries which were incorporated in order to represent gasoil liquid, gasoil vapour and gasoline vapour species, the evaporation model calculations and source terms, as well as the implementation of the cracking reaction rate. All UDFs are designed to work on serial/parallel and 2D/3D versions of the software.

3. Results and Discussion

The validation of the phase change CFD model for its use in this study is presented in the Appendix section.

In this section, a parametric investigation on droplet-particle collision dynamics for the operating conditions resembling those exhibiting in a real FCC injection zone is made. Table 2 presents the constant operating conditions used in all parametric computational runs conducted (based on Figure 1), while in Table 3, the total eight (8) simulation cases are presented, along with the main parameters studied. Contact angle was assumed to take a value of 100^o degrees. To the best of authors' knowledge no experimental values regarding the contact angles of heavy hydrocarbons on catalytic particles were tracked in the open literature. Nevertheless, its effect on the numerical results, for the range of conditions examined in this paper, is regarded to be small and influential only for the cases where a direct contact of the liquid phase with the solid one is calculated. The impact velocity, takes two different values, i.e. 15 and 30 m/s, which represent low and moderate impact energy collisions. Droplet impact velocity represents the relative velocity between liquid droplets-catalytic particles near the injection area; these are typical values for an operating FCC unit based on literature findings as reported in the Introduction section of the paper. The particle temperature ranges between 800K and 1000K,

which covers the entire spectra of catalyst temperatures inside the bed, from their inlet till steady-state condition has been established. Finally, the droplet to particle size ratio (DTP) is set equal to either 1 or 2, thus representing two typical injected droplet sizes selected from the range (DTP= 0.67 – 6.67, [6, 8, 17]) and identifying its relative importance relative to the effects of temperature and impact velocity variations. For DTP values higher than two, the solid-liquid contact time is expected to increase, which will probably affect the deformation of the droplet as well as the gasoline yields. Investigation of higher DTP values is out of the scope of the present work.

P_{oper} (Pa)	T_{drop} (K)	T_{gas} (K)	D_p (μm)	Θ (°)
202,650	550	800	75	100

Table 2. Constant operating conditions for all cases.

Case No.	DTP	Uo	Tp	We	Re	Refinement Levels
1	1	15	800	4266	2272	3
2	1	15	1000	4266	2272	3
3	1	30	800	17062	4544	3
4	1	30	1000	17062	4544	3
5	2	15	800	8531	4544	2
6	2	15	1000	8531	4544	2
7	2	30	800	34124	9088	2
8	2	30	1000	34124	9088	2

Table 3. Cases investigated for droplet-partile collisions in FCC reactor injection zone.

The Weber number in all cases is extremely high, as the surface tension coefficient in such conditions (high temperature) is very low. Therefore, the effect of surface tension on the progression of the phenomenon is expected to be insignificant, though it has been considered for reasons of completness.

3.1 Computational domain and Boundary conditions

The 2D axisymmetric computational domain/mesh which was used for the cases presented above, along with the applied boundary conditions, is shown in Figure 3a. Particle is assumed to be stationary. In reality, when the droplet impinges onto the moving particle, momentum is transferred. However, in this work, this momentum exchange is neglected, as this would require not only the use of more complex

models needed to capture the simultaneous motion of the solid particle (such as rigid solid body motion and mesh deformation or the Immersed Boundary Method or other) but also would add the direction of impact as an additional variable. The semi-circular circumference of the particle was split into 40 divisions, achieving a cell width of approximately 5.89 μm in the initial coarse grid. The same cell width was used in all cells inside the circular zone with dimensions shown in Figure 3a, while in the rest of the domain the cell width was approximately 20μm. After a parametric study on what should be the discretization of the droplet radius, it was concluded that a cpR (cells per drop Radius) equal to around 51 (achieved with local refinement) refines quite well the droplet keeping at the same time affordable the required computational cost, while simultaneously dense enough to capture the phenomenon of droplet levitation (gas layer resolved within 1-2cells) for the operating conditions, where this is expected to occur (as seen in Figure 5). Denser grids (cpR=144) as applied for the validation cases, would result in too expensive runs for 2D simulations, without a corresponding significant increase in the accuracy of the simulation. Additionally, given the fact that for certain cases 3D simulations may be required, as will be explained in following sections, the choice of cpR equal to 144 would not be feasible to run with the present available allocated computational resources. The total number of triangular cells in the beginning of the simulations was 8,436 and 15,142 for Cases 1-4 and 5-8 respectively, while the maximum number of cells were approximately 14,000 and 22,000 respectively.

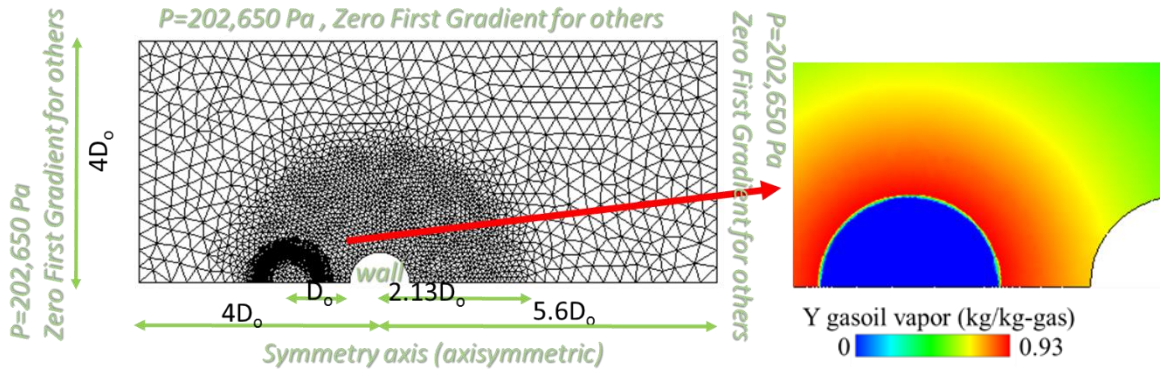

Figure 3. a) Computational domain used for simulated cases. b) Gasoil vapour mass fraction initialization.

The positioning of a droplet inside a hot gaseous medium, with T_g - T_l= 250K, without an a priori saturated gas layer around the droplet results in high evaporation rates during the first stages of the simulation until the droplet interface is saturated. The derived large density gradients formed in the

small space of 1-2 cells (interface) around the droplet, increase in turn the induced velocity field which diverges. Therefore, a pre-initialization step of gasoil vapour field around the droplet is required, in order to avoid numerical divergence. The latter is presented in Figure 3b, while it is of importance to stress out that this saturated vapour layer exists as well in any real physical problem at a distance close to droplet interface. In numerical terms, the interface is assumed to be saturated, while the concentration of gasoil vapour decreases moving radially away from the droplet interface, following a simple custom function of type

$$Y(\tilde{d}) = 1-(1-Y_{sat})\left(\frac{1}{1-Y_{sat}}\right)^{1-1/\tilde{d}}, \quad \tilde{d} = MAX(d/R_o, 1) \qquad (11)$$

where d is the distance of each cell from droplet center. Based on performed numerical tests, the initial gasoil vapour distribution given by this function does not affect the gasoline yield if another function or constant initial value is used.

3.2 Results

In the following section, all results are presented in non-dimensional form, so that the comparison among all cases is direct and general conclusions can be drawn. Non-dimensional time τ ($=tu_oD_o$) is set to zero at the time instant of impact.

3.2.1 DTP=1

In Figure 4, the evolution of droplet shape during the impingement process is depicted for Cases 1 (top) and 3 (bottom), while in Figure 5 the same results are presented for Cases 2 and 4. In these Figures low velocity impact cases (top) are separated from high impact velocity ones (bottom) by the symmetry axis. The corresponding contour of the produced gasoline lump mass fraction is also shown.

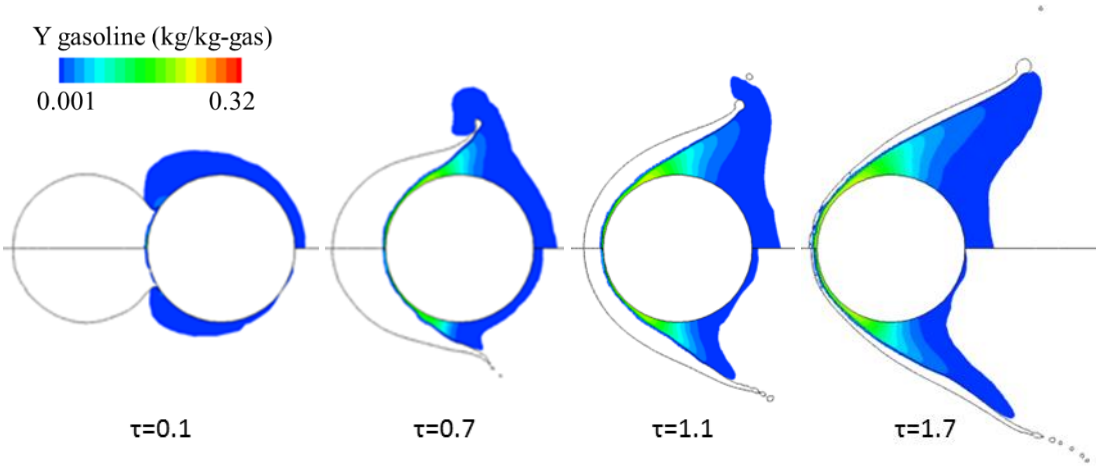

Figure 4. Effect of impact velocity on collision outcome for wall temperature 800K, Case1 (top), Case3 (bottom). Contour of the produced gasoline mass fraction (kg-gasoline/kg-gas).

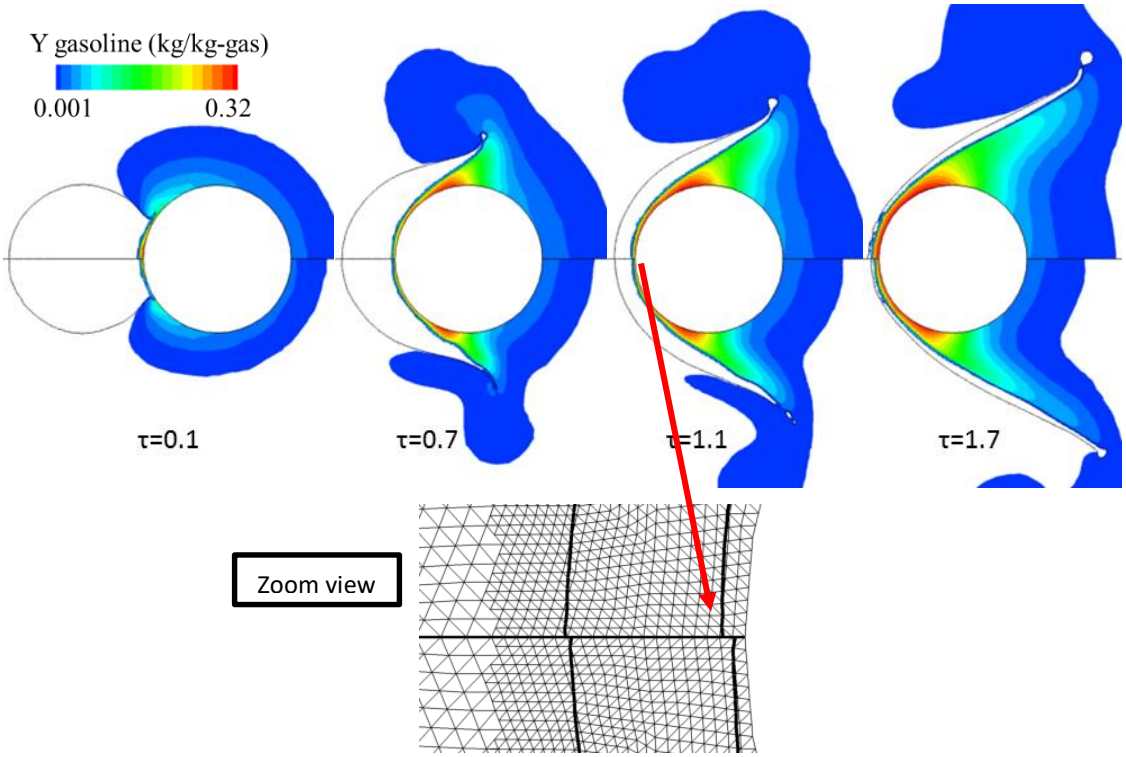

Figure 5. Effect of impact velocity on collision outcome for wall temperature 1000K, Case2 (top), Case4 (bottom). Contour of the produced gasoline mass fraction (kg-gasoline/kg-gas). Close up to the resolved gas layer cell thickness.

By firstly comparing Figure 4 and Figure 5, it is observed that the effect of temperature on the final hydrodynamic outcome of the whole phenomenon is minor, meaning that in all Cases 1-4, the droplet

impacts the solid particle (τ=0.1), then deforms as it moves along the particle periphery (τ=0.7), and forms a liquid sheet that moves away from the particle surface (τ=1.1). In other words, the macroscopic result of collision under different impact velocities in the range of 15-30 m/sec remains almost the same, irrespective of the catalytic particle temperature. This liquid sheet becomes very thin (τ=1.7) and finally (τ>2) breaks up into numerous satellite droplets (torous shapes for 2D simulations), as shown in Figure 6 for Cases1-4. In this study, the main results are presented for dimensionless time below τ=2, because the 2D axisymmetric simulations are deemed unreliable to simulate phenomena of break-up such as the ones presented in Figure 6. This Figure is presented only for revealing that after τ=2, the deformed liquid shape is expected to break-up from its expanding rim, into numerous satellite droplets. In Part II of this paper, it is shown that 3D simulations are more reliable after this non-dimensional time because the 2D axisymmetric approach can only predict torus break up while in fact the lamella breaks up in multiple droplets.

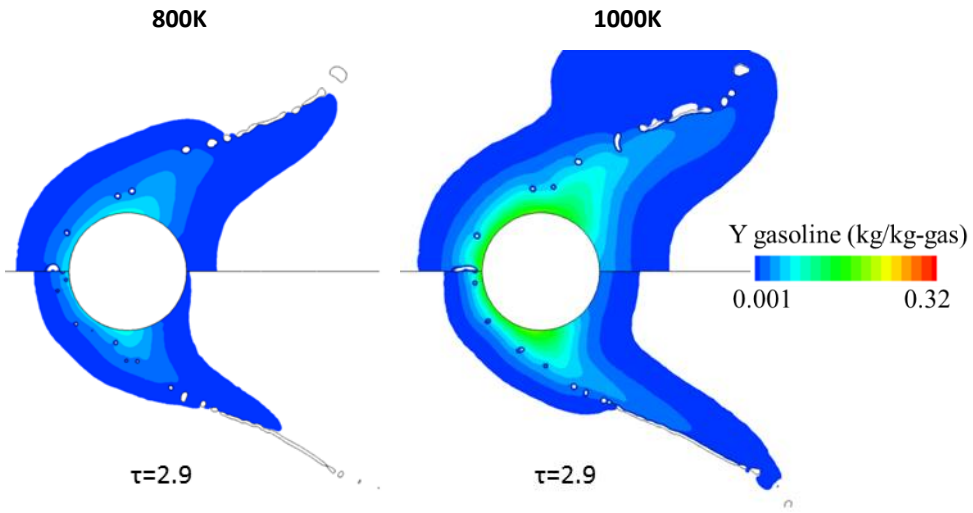

Figure 6. Breakup of the liquid sheet for cases 1-4. Case 1 (up-left) - Case 2 (up- right) – Case 3 (bottom-left) – Case 4(bottom-right). Contour of the produced gasoline mass fraction (kg-gasoline/kg-gas).

Focusing now on the effect of impact velocity on the collision outcome, apart from small changes observed in the liquid sheet thickness and shape, significant differences are observed in the formed gas layer thickness that levitates the droplet in all Cases 1-4. This gas layer is formed due to high evaporation rates and is reinforced by an upward gas motion induced by temperature gradient (hot catalyst) and density gradient (light gasoline production) resulting in pushing the droplet away. In Figure

7b, the non-dimensional gas layer thickness is plotted against the non-dimensional time of the impingement phenomenon for cases 1-4.

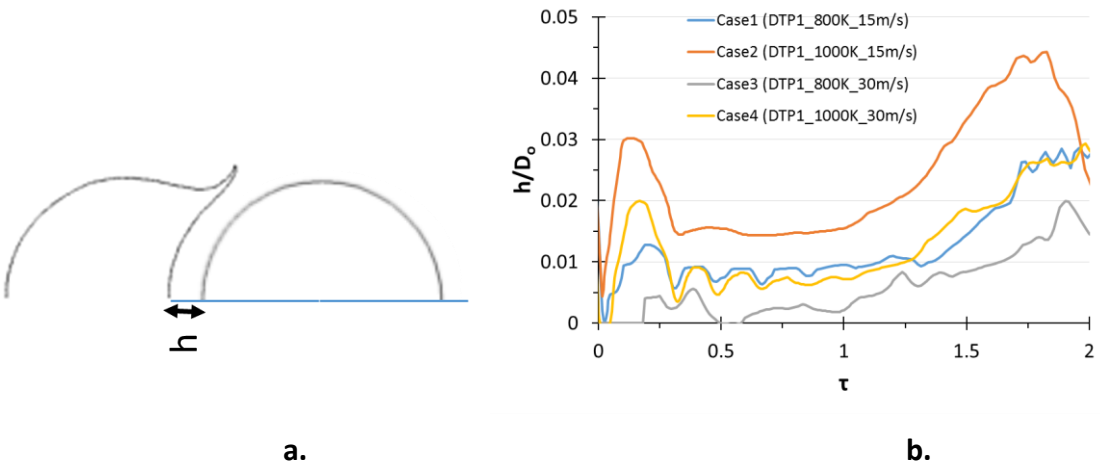

Figure 7. a) Definition of the vapour layer thickness at the impact point, b) Temporal evolution of the vapour layer thickness at the impact point for Cases 1-4.

For the same catalyst temperature, as the kinetic energy of impact gets higher, the gas layer is more difficult to form since the drop momentum is higher (see Figure 5 zoom view), thus the smaller values observed in Figure 7. Additionally, as the catalyst temperature increases, for the same impact velocity, the cracking reaction is promoted through Arrhenius kinetics (eq. 10), thus more gasoline is produced which poses a greater burden to the droplet coming in contact with the catalyst, justifying the thicker gas layer presented in Figure 7. The significant parameters that affect the thickness of the gas layer and thus the space provided for the catalyst to be active in cracking terms are the initial drop kinetic energy, viscous dissipation and the catalyst temperature. Moreover, from the CFD results it is observed that after the droplet impacts the catalytic particle, for a significant period of time ($\tau<0.5$), the drop initial kinetic energy pushes the droplet forward, while the evaporation of gasoil vapor and the formation of gasoline try to push it away. This back and forth motion is clearly seen in Figure 7 in the initial ($\tau<0.5$) perturbations of the gas layer thickness, while also in Figure 4 and Figure 5, at $\tau=0.7$, it is observed that for the high impact velocity cases, the formation of (wavy like) perturbations, located at the inner surface of the liquid sheet, are clearly seen. These perturbations, as will be shown in Part II of this paper, are numerical artefacts that are eliminated when the same case is solved in 3D domain.

Overall, in all cases (1-4), the gas layer thickness stabilizes for $\tau>0.5$ at a value of approximately 0.8-1.5% of the initial droplet diameter, i.e. in absolute values 0.6-1.125μm (resolved by 1-2 numerical cells, as

shown in Figure 5). In Case 3, the droplet initially touches the catalyst. The initial perturbation of the liquid phase imposed by this contact, is expected to cause the earlier breakup of the formed lamella; this is evident by comparing Figure 4 (bottom) to Figure 5 (bottom), corresponding to Case 4. The only difference between these cases is the particle initial temperature (800 vs 1000K) which does not influence the droplet mean temperature (maximum temperature difference of 1K between Cases 3,4 depicted in Figure 14); therefore the droplet properties (surface tension, viscosity etc) do not change significantly and subsequently the initial droplet-catalyst contact can be held responsible for the earlier breakup. The gas layer formed justifies the comments of [6, 15] that film boiling regime is the principal regime of FCC operation.

Another interesting aspect that is observed and is shown schematically in Figure 8 are the vortex rings induced at the vicinity of the expanding lamella rim, one on the top of the liquid sheet (outer ring) and a second one on the bottom (inner ring), expanding up to the particle wake region, during the impact process. In this Figure, the gasoil vapour mass fraction is also presented. For higher initial drop kinetic energy (Figure 8b), the inner vortex ring bends slightly the deforming liquid sheet towards the catalytic particle. In general, as the axial momentum of the droplet overweighs the upward motion, the liquid sheet stays closer to the particle. This can be seen in Figure 4 for the dimensionless times of 0.7 and 1.1.

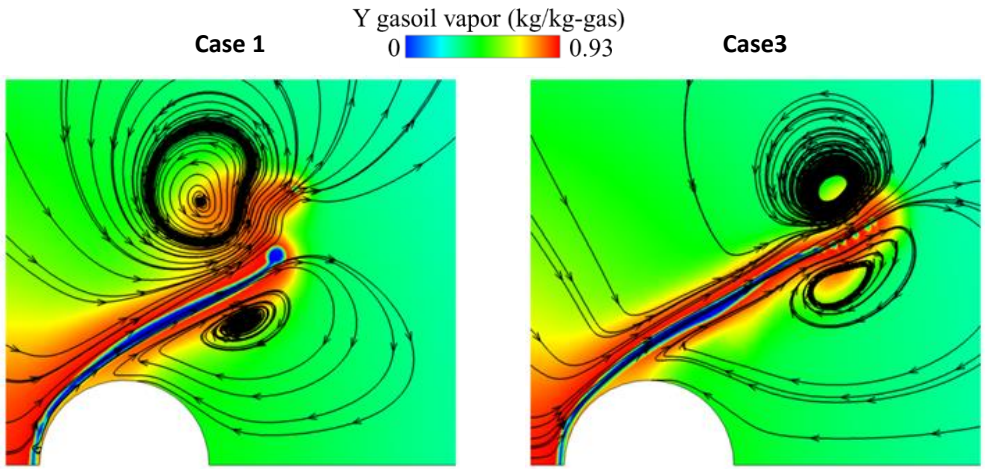

a. b.

Figure 8. Vortex rings formed during impingement for a) Case1 (low impact velocity) and b) Case3 (high impact velocity) for wall temperature 800K at τ=1.7. Figures coloured with gasoil vapour mass fraction (kg-gasoil vapour/kg-gas, blue colour denotes zero gasoil vapor, i.e. pure liquid phase).

In Figure 9 the percentage of gasoil converted to gasoline, as well as the total reaction rate, i.e. the total number of moles of gasoline generated per second throughout the process are presented.

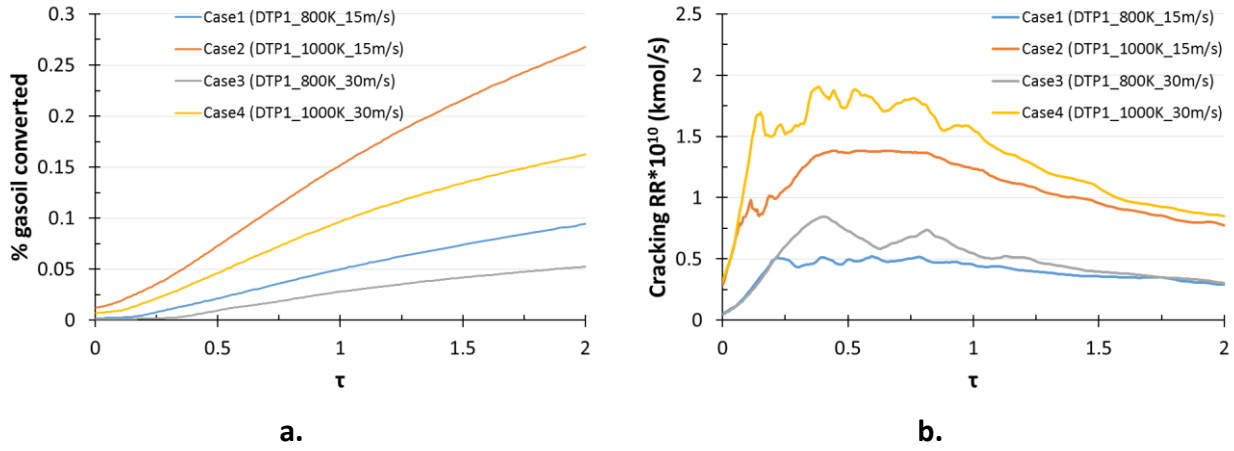

Figure 9. a) Percentage of gasoil converted to gasoline yield (kg-gasoline/kg-liq %) and b) cracking reaction rate, both plotted against non-dimensional time for Cases1-4.

It is clear that the high catalyst temperature impacts outweigh the low catalyst temperature ones in both diagrams as was clearly observed in Figure 4 and Figure 5. This is due to the thicker gas layer, which results from higher reaction kinetics. The resulting higher gas layer thickness offers more space for reactions to occur and promotes the production of higher gasoline yields. It is important to notice the total gasoline yields are 2.5-3 times higher for high catalyst temperature catalysts (Figure 9a).

Focusing now on the effect that the impact velocity has over the total yield of gasoline lump specie, a very interesting phenomenon is observed. Given the same catalyst temperature, although the cracking reaction rate is higher for the high impact velocity cases, the total gasoline yield is lowering, which is again explained by the gas layer thickness differences between these cases (lower impact kinetic energy results in thicker layer). Moreover, the real contact time for the low impact velocity cases is much higher, thus higher gasoline yields are expected. As a matter of fact, low impact velocity promotes yield by 1.5-2 times, in comparison to high impact velocity ones.

3.2.2 DTP=2

The results for the double sized droplets are presented in Figure 10 and Figure 11 for Cases 5,7 and Cases 6,8 respectively. Overall, similar trends to the DTP=1 Cases 1-4 cases are observed, meaning the droplet deforms into a liquid sheet that tends to move away from the particle surface. In high impact

velocity Cases 7 and 8 the liquid mass is entrained by the inner vortex ring, resulting in its sucking inside the wake region of the catalytic particle (downstream the catalyst), towards the symmetry axis.

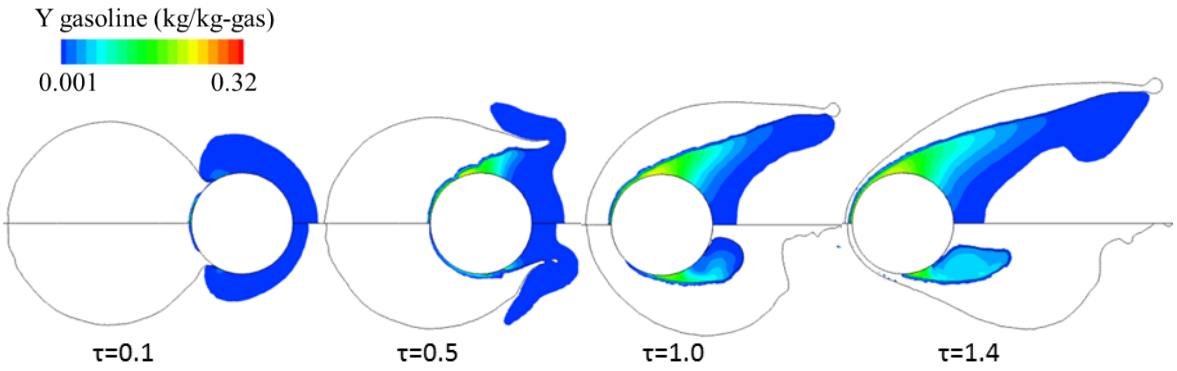

Figure 10. Effect of impact velocity on collision outcome for wall temperature 800K, Case5 (top), Case7 (bottom). Contour of the produced gasoline mass fraction (kg-gasoline/kg-gas).

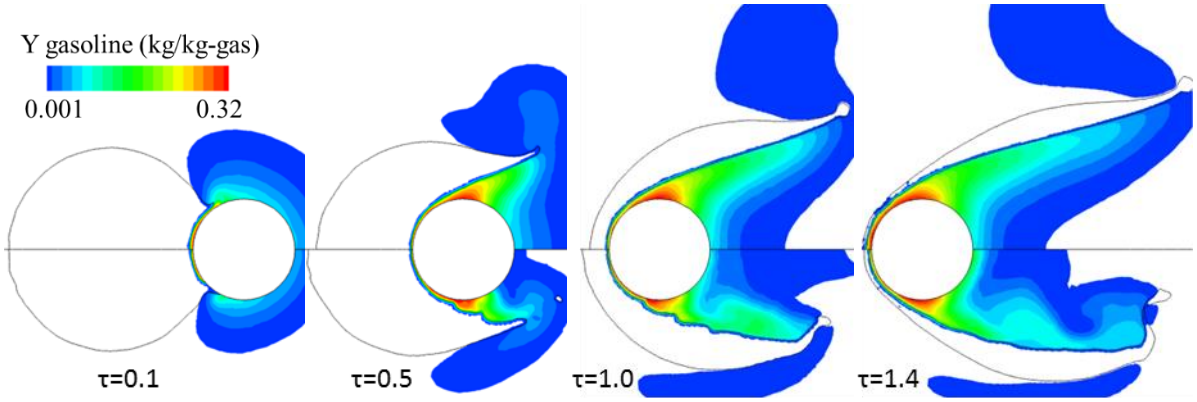

Figure 11. Effect of impact velocity on collision outcome for wall temperature 1000K, Case6 (top), Case8 (bottom). Contour of the produced gasoline mass fraction (kg-gasoline /kg-gas).

More specifically in Case 7, where a liquid shape is formed close to the symmetry axis, it can be doubted if this form is representative of real conditions, since three dimensional effects occur. In the following 3 dimensional runs (Part II), this is investigated. The perturbations on the inner side of the liquid sheet are visible both for low impact velocity Case 5 (τ=0.5), as well as for high impact velocity Case 8 (τ=0.5).

When the droplet is bigger, its initial kinetic energy is higher than the smaller one, which limits the formed gas layer thickness. This is observed in Figure 12, where the temporal evolution of the vapour layer thickness size is presented for Cases 5-8.

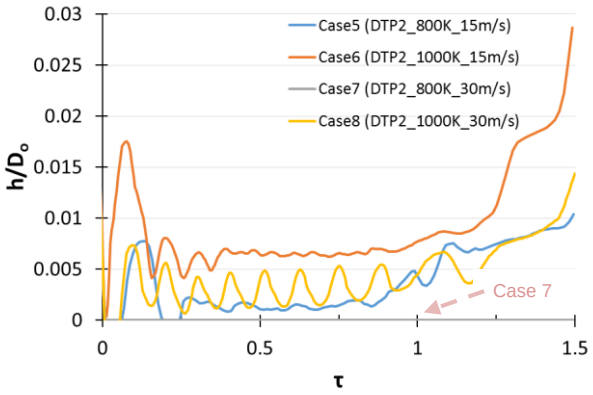

Figure 12. Temporal evolution of vapour layer thickness at impact point for Cases 5-8.

It is evident that now the non-dimensional vapour layer thickness stabilizes at a smaller value than in Cases 1-4, i.e. around 0.2-0.6% of the initial droplet diameter, a value of approximately 0.3-0.9μm (resolved by almost 1 cell). In Case 7, which is the worst case scenario in terms of yield efficiency (low catalyst temperature and high drop kinetic energy), the droplet is in direct contact with the particle throughout the whole collision phenomenon. Such conditions occur within the injection zone of industrial FCC reactors, owed to the fact that liquid droplets are mostly characterized by high DTP values [6, 8, 17] and high velocities, resulting in long contact times with the catalytic particles, and subsequent higher probability of liquid-pore blocking and catalyst deactivation, which is a phenomenon experienced in industrial scales [12].

Finally, the results for the gasoil conversion, as well as total reaction rate of cracking for Cases 5-8 are presented in Figure 13. Similar trends are observed for all four (4) examined cases. The reaction rate values for cases 5-8 are higher than the corresponding of cases 1-4, while in contrast the percentage of gasoil converted is much lower. The higher reaction rates are attributed to the higher coverage of particle area in the case of double sized droplet, while the lower conversion is owed to higher liquid mass which is used to non-dimensionalize the gasoil conversion yield.

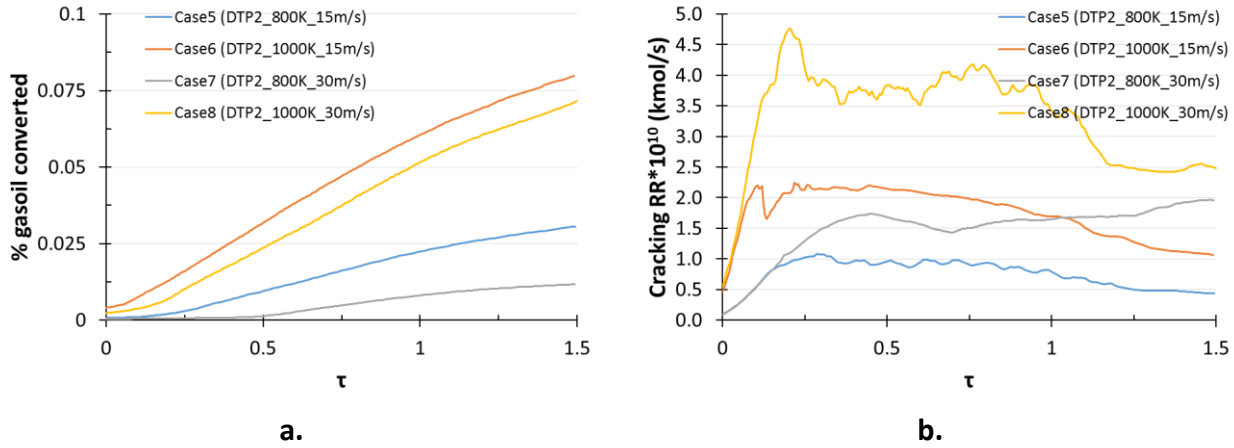

Figure 13. a) Percentage of gasoil converted to gasoline yield (kg-gasoline/kg-liq %) and b) cracking reaction rate, both plotted against non-dimensional time for Cases5-8.

Based on all cases simulated in this work, where the interest is turned towards limiting the possibility of liquid pore blocking and improving gasoline yields, Case 7 was found to represent the worst case scenario. The operating conditions of this case are actually the most commonly found in current FCC operating units. On the other hand, Case 2 acts as the best case scenario. Additionally, a further finding of this study is that gasoil conversion can be well linked with the direct solid-liquid contact which in our case is estimated by the predicted gas layer thickness formed in between the impacting droplet and the catalyst. It was observed that as the temperature of the catalyst increases or the initial drop kinetic energy decreases, the gas layer is formed more easily, and therefore the possibility of liquid pore blockage decreases. Another way to estimate solid-liquid contact would be to measure the percentage of wall area which is actually covered in liquid as in [34]. Finally, the best/worst case scenarios refer only to the operating conditions investigated.

The present study can be further applied for simulating additional range of values for the parameter of DTP (higher values actually appear in industry), which is an important controlling physics variable in terms of catalyst pore blockage mechanism and catalyst deactivation. Further numerical developments that can be made include the inclusion of momentum exchange between droplet/catalyst during collision and the investigation of the exact porous geometry.

3.3 Discussion

What matters in most large scale models, concerning the outcome of droplet-particle collisions, is the state the droplet will be after it hits a particle. In Figure 14, the droplet mass, as well as the average droplet temperature are plotted against time. In an FCC reactor, a droplet after its collision with an

equally sized particle loses up to 5% of its initial mass, while for double sized droplets the decrease is in the range of 2%. After the breakup of the liquid sheet into secondary droplets, for a non-dimensional time higher than 2, the liquid mass decrease is expected to be higher. It should be pointed out that the droplet mass loss in the cases with DTP=2, when expressed in (kg), is much larger when compared to cases with DTP=1, since in the former cases the droplet volume is 8 times higher than the latter ones. The temperature of the liquid that is travelling downstream the catalytic particle, is almost constant (decrease less than 2.5K) during the whole evolution, owed to high evaporation rates, which tend to keep the droplet temperature at a constant temperature state. In Case7 particularly, due to the direct contact between drop-particle the mean droplet temperature is expected to rise, as shown in Figure 14b.

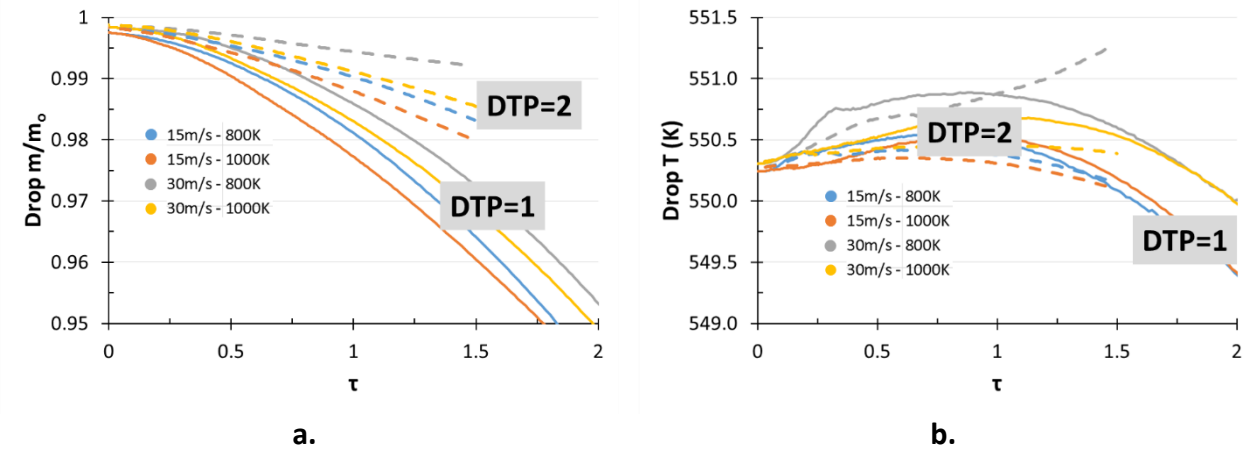

Figure 14. Droplet a) mass and b) temperature evolution for all cases, (solid lines-DTP1, dashed lines-DTP2).

The direction that the liquid mass will follow after its collision can be found by the drop maximum radial deformation, which is presented in Figure 15 for all cases examined (DTP=1, 2). It is evident that for high velocity and double sized droplet impacts, the remaining liquid mass will in fact stay closer to the drop-particle axis. As for Case7 in particular, the droplet will perform a “copy” impingent, meaning it will impact the following catalytic particle downstream with almost a spherical shape, as depicted in Figure 10, τ=1.4. A D_y/D_o limiting value equal to around 1.25, differentiates “copy-impingement” from skirt-sheet formation, as it was named in the work of Gac and Gradon [14].

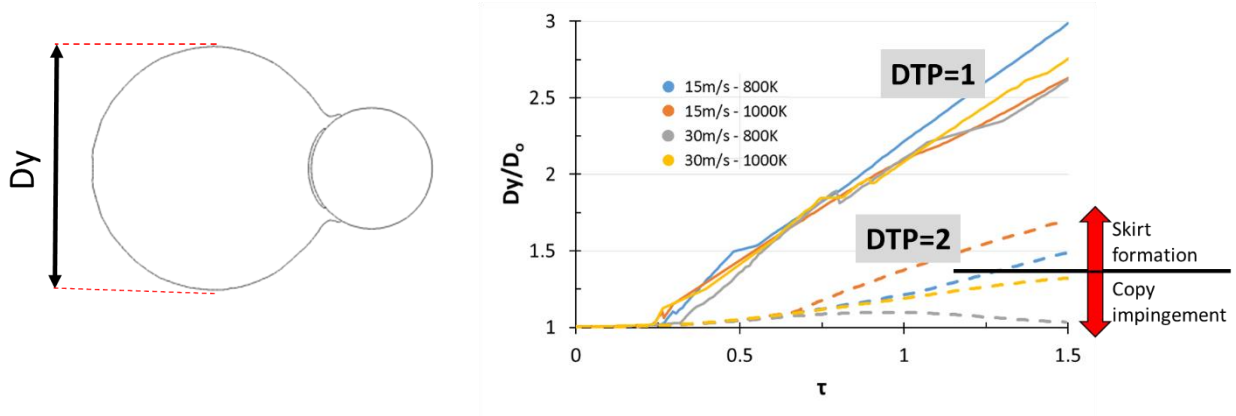

Figure 15. a) Definition of drop maximum radial deformation, b) Temporal evolution of the maximum radial deformation for all Cases 1-8 (solid lines-DTP1, dashed lines-DTP2).

The mass weighted mean drop velocity is also very important. In Figure 16 it is shown that for DTP=1, the post impact secondary droplets will have approximately 75% of their mother droplet impact velocity, while for DTP=2, either the secondary droplets or the "copy" one will move at 90-95% of their mother droplet impact velocity.

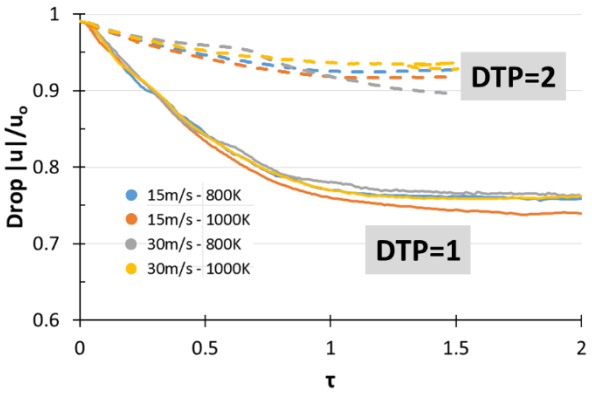

Figure 16. Droplet mass weighted velocity non-dimensionalized with impact velocity for all cases1-8, (solid lines-DTP1, dashed lines-DTP2).

In Figure 17, the liquid film height for all cases simulated (Cases 1-8) at the impact point on the symmetry axis is presented. The similarity in the trend of all lines reveals the dimensionless character this quantity follows during such type of impingements, as is also stated in isothermal works [42, 43].

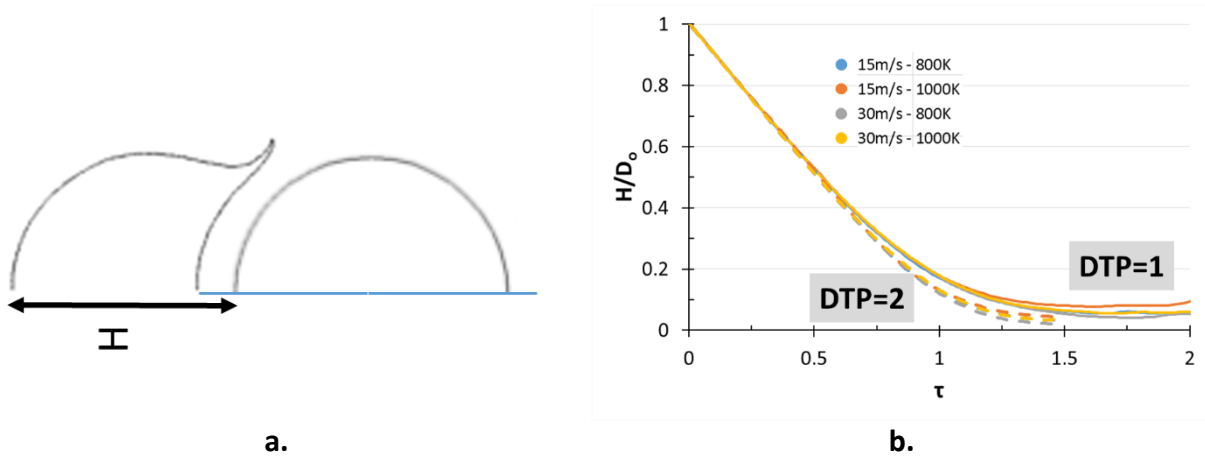

Figure 17. a) Definition of liquid film thickness, b) Temporal evolution of the non-dimensional liquid film thickness for all Cases 1-8 (solid lines-DTP1, dashed lines-DTP2).

4. Conclusions

In this study the Navier-Stokes equations, along with the energy conservation, transport of species equations and the Volume of Fluid two phase flow methodology are used for the investigation of droplet-particle collisions at conditions relevant to those realised in the injection zone of Fluid Catalytic Cracking (FCC) reactors. A phase change model and a simplified 2-lump scheme were implemented in the numerical framework so as to incorporate the vaporization process and surface cracking reactions respectively. Dynamic local grid refinement technique was also applied for the minimization of computational cost. The resulting numerical model was validated for numerous conditions of standard single droplet evaporation regimes, i.e. in a hot gas medium and droplet impingement onto hot flat solid surface under film boiling and droplet heating regimes. Afterwards, it was used for the investigation of FCC collision dynamics with basic controlling parameters investigated being, a) the catalyst temperature, b) the initial drop impact velocity and c) the droplet-to-particle size ratio. It was shown that the best case scenario concerning conversion yields and potential liquid pore blocking prevention corresponds to gasoil droplets of similar to the catalytic particle size, very hot catalysts (at 1000K) and low impact velocities (15m/s). In this way, the levitation of the droplet is promoted, which gives enough room for catalytic reactions to occur and at the same time preventing catalyst pores not to come in contact with non-evaporated liquid and thus pores blogging. This rapid phenomenon, with time-scale in the order of micro-seconds may in fact influence the total yield and selectivity of light-gas products, as well as catalyst deactivation, in FCC reactors.

5. Acknowledgements

The present work was funded by the Marie Curie Fellowship (FP7-PEOPLE-2012-IEF) with Grant Agreement number 329500 funded by the European Commission entitled as “Non Flat Impingement—Droplet Impingement on Non-flat Surfaces”.

6. Appendix. Validation of CFD phase change model

The validation of the phase change model is divided in two parts, firstly evaluate the behavior of the model in single drop evaporation and secondly test its performance in real cases similar to this study (hot wall impingement).

For the initial validation of the phase change model under operating conditions concerning the present study (evaporation of free flowing/suspended heavy hydrocarbons, with more than 20 carbon atoms, at high gas temperatures in the range of 800-100K), scarce experimental material can be found in literature. In the work of Wong and Lin [44], concerning n-decane droplets, the ambient temperature reaches 1,000K (as in this study), however the gas flowing towards the suspended droplet affects evaporation. For the correct simulation of this phenomenon, in terms of CFD, the coupled solution of the phase change model with flow equations (as in Strotos et al. [45]) is needed, a task considered to be computationally expensive for the framework of this study, given the Courant restrictions, since this phenomenon lasts many seconds. On the other hand in Nomura et al. [46], gas temperature varies between 400 and 1000K and gas pressure between 0.1-5MPa for the case of n-heptane droplet evaporation under microgravity conditions, while for these specific conditions gas velocity was considered to be of minor importance. Therefore, it was decided this work to be used for the validation of the phase change model as standalone, without its coupling with flow equations (pure diffusion). It should be pointed out that in their work, Nomura et al. [46] mention that droplet diameter ranges between 600 and 800 μm, initially set at room temperature. In this study a mean 700μm droplet is initialized at 293.15K in the domain presented in Figure 18. The initial grid consists of 2,682 elements, while 4 levels of local refinement are additionally applied. The size of the domain is very large, so that the temperature of the gas phase cannot not be affected (cooled-down), due to heat transfer of hot gas to the cold droplet.

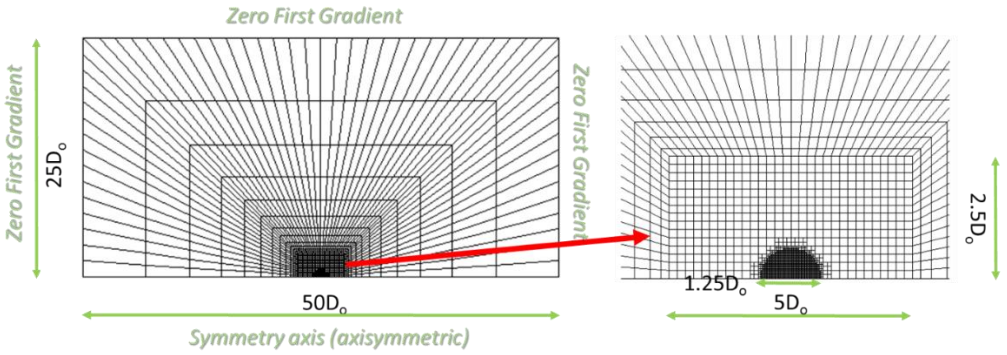

Figure 18. Computational domain used for the validation of the CFD evaporation model in single droplet evaporation (pure diffusion).

In Figure 19 the results of the phase change model for the temporal evolution of the squared droplet diameter are compared against the experimental values of Nomura et al. [46]. The evaporation model is deemed to be reliable and can be used for the investigation of heavy hydrocarbons, applicable in this study. Additionally, the average droplet temporal evolution is as well depicted, for which no experimental data were given.

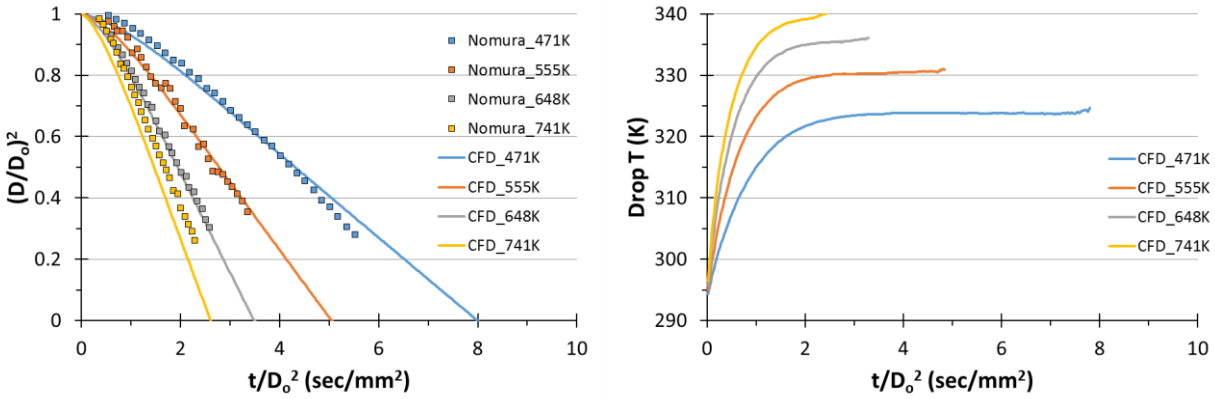

Figure 19. Validation of the CFD phase change model against the experiments of Nomura et al. [46] for n-heptane droplets evaporating at 101,325 Pa.

For the second validation, the phase change model needs to be tested in cases where the flow equations are solved. The behaviour of the numerical model in the case of droplet impingement onto a heated wall under droplet heating (direct solid-liquid contact) and film boiling conditions, both of which are of interest to this study, needs to be evaluated. The experimental observations of Qiao and Chandra [47] serve this goal; respective properties are presented in Table 4. Although in [16, 48] the authors

present experimental data for drop impact onto a heated particle, these data were not used for validation since they only refer to film boiling conditions (in [16], although cases for lower surface temperatures exist, data are not adequate for validation).

Case No (Regime)	Exper	species	D_0	u_0	$T_{dr,0}$	T_g	u_g	T_w	cpR	θ(°)
V1 (droplet heating)	[47]	C_7H_{16}	1.5	0.8	298	298	0	451	144	100
V2 (droplet heating)	[47]	C_7H_{16}	1.5	0.8	298	298	0	463	144	100
V3 (Film Boiling)	[47]	C_7H_{16}	1.5	0.8	298	298	0	483	144	100

Table 4. Test cases investigated for the validation of the CFD phase change model in drop impact on a heated wall.

Figure 20 presents the applied CFD domain and boundary conditions, while the derived numerical results for both the non-dimensional droplet spreading and liquid height are shown in Figure 21 and compared against the experimental values of Qiao and Chandra [47].

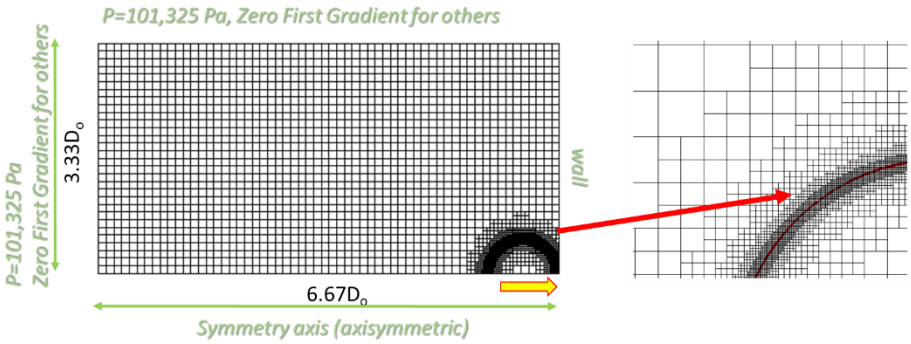

a. b.

Figure 20. a) Computational domain (grid=30x60 cells) used for the validation of the CFD model in hot wall impingement cases, b) 5 levels of local refinement used in order to resolve the thin vapour layer.

The cpR number used in these cases is very high (144), so that the vapour layer thickness can be resolved explicitly and not through the coupled solution of an additional equation for the vapour layer thickness as in Harvie and Fletcher [49] and Ge and Fan [15]. CFD results seem to be in good agreement with the experimental values.

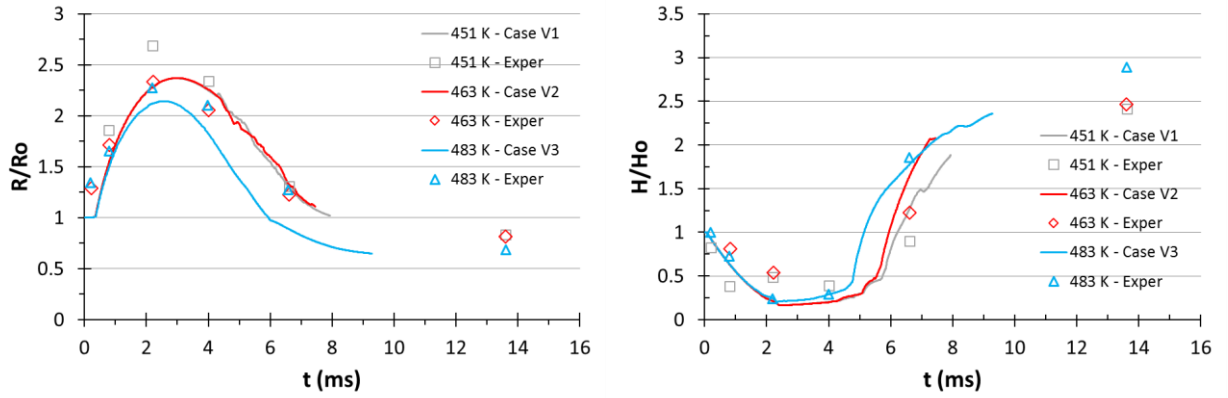

Figure 21. Temporal evolution of a) maximum non-dimensional radius and b) maximum non-dimensional height of spreading droplet for the 3 cases examined against experimental values of Qiao and Chandra [47].

In Figure 22, contours of temperature and n-heptane vapour mass fraction are presented for selected time instants throughout the phenomenon. In the first two cases, a vapour bubble is formed in the centre of the spreading droplet.

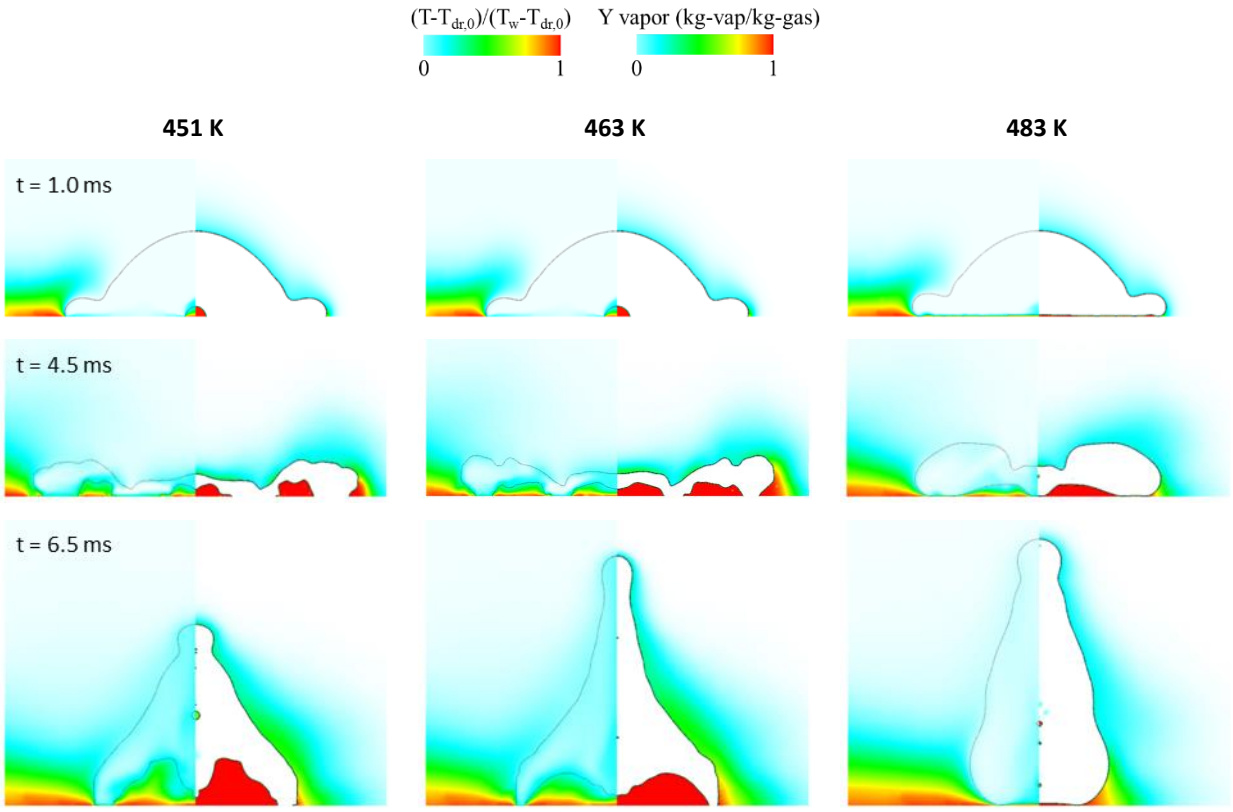

Figure 22. Temporal evolution of drop deformation for validation cases of impingement on a heated wall. Images split in two sides, left side-non-dimensional temperature, right side-heptane vapour mass fraction (kg-vap/kg-gas).

This bubble grows widely and finally merges with the bubble formed under the retracting droplet rim. In the third case, the levitation of the droplet due to the appearance of a vapour layer is observed. The numerical model is able to resolve this vapour layer formed in-between the droplet and the solid surface, thus it can be used as a first validated step for the main scope of the paper.

7. REFERENCES

1. Lopes, G.C., et al., *Three-dimensional modeling of fluid catalytic cracking industrial riser flow and reactions.* Computers & Chemical Engineering, 2011. **35**(11): p. 2159-2168.
2. Li, T., et al., *Numerical investigation of FLUID COKING™ units, Part I: Hydrodynamics of a scaled cold flow model.* The Canadian Journal of Chemical Engineering, 2012. **90**(2): p. 442-456.
3. Ahsan, M., *Prediction of gasoline yield in a fluid catalytic cracking (FCC) riser using k-epsilon turbulence and 4-lump kinetic models: A computational fluid dynamics (CFD) approach.* Journal of King Saud University - Engineering Sciences, (0).
4. Chang, J., et al., *Computational investigation of the hydrodynamics, heat transfer and kinetic reaction in an FCC gasoline riser.* Chemical Engineering Science, 2014. **111**(0): p. 170-179.
5. Wu, C., et al., *CFD–DEM simulation of gas–solid reacting flows in fluid catalytic cracking (FCC) process.* Chemical Engineering Science, 2010. **65**(1): p. 542-549.
6. Nayak, S.V., S.L. Joshi, and V.V. Ranade, *Modeling of vaporization and cracking of liquid oil injected in a gas–solid riser.* Chemical Engineering Science, 2005. **60**(22): p. 6049-6066.
7. Theologos, K.N., A.I. Lygeros, and N.C. Markatos, *Feedstock atomization effects on FCC riser reactors selectivity.* Chemical Engineering Science, 1999. **54**(22): p. 5617-5625.
8. Gao, J., et al., *Simulations of gas-liquid-solid 3-phase flow and reaction in FCC riser reactors.* AIChE Journal, 2001. **47**(3): p. 677-692.
9. Chang, S.L. and C.Q. Zhou, *Simulation of FCC riser flow with multiphase heat transfer and cracking reactions.* Computational Mechanics, 2003. **31**(6): p. 519-532.
10. Chang, J., et al., *Computational investigation of hydrodynamics and cracking reaction in a heavy oil riser reactor.* Particuology, 2012. **10**(2): p. 184-195.
11. Behjat, Y., S. Shahhosseini, and M.A. Marvast, *Simulation study of droplet vaporization effects on gas–solid fluidized bed.* Journal of the Taiwan Institute of Chemical Engineers, 2011. **42**(3): p. 419-427.
12. Huang, Z. and T.C. Ho, *Effect of thermolysis on resid droplet vaporization in fluid catalytic cracking.* Chemical Engineering Journal, 2003. **91**(1): p. 45-58.
13. Sadeghbeigi, R., *Fluid Catalytic Cracking Handbook: An Expert Guide to the Practical Operation, Design, and Optimization of FCC Units*2012: Butterworth-Heinemann.
14. Gac, J.M. and L. Gradoń, *Lattice-Boltzmann modeling of collisions between droplets and particles.* Colloids and Surfaces A: Physicochemical and Engineering Aspects, 2014. **441**(0): p. 831-836.
15. Ge, Y. and L.-S. Fan, *Droplet–particle collision mechanics with film-boiling evaporation.* Journal of Fluid Mechanics, 2007. **573**: p. 311-337.
16. Mitra, S., et al., *Droplet impact dynamics on a spherical particle.* Chemical Engineering Science, 2013. **100**(0): p. 105-119.
17. Patel, R., et al., *Effect of injection zone cracking on fluid catalytic cracking.* AIChE Journal, 2013. **59**(4): p. 1226-1235.

18. Ancheyta, J., *Modeling and Simulation of Catalytic Reactors for Petroleum Refining*2011: Wiley.
19. Jakobsen, H.A., *Chemical Reactor Modeling: Multiphase Reactive Flows*2008: Springer.
20. Weekman, V.W. and D.M. Nace, *Kinetics of catalytic cracking selectivity in fixed, moving, and fluid bed reactors.* AIChE Journal, 1970. **16**(3): p. 397-404.
21. Yen, L.C., R.E. Wrench, and A.S. Ong, *Reaction kinetic correlation equation predicts fluid catalytic cracking coke yields.* Journal Name: Oil Gas J.; (United States); Journal Volume: 86:2, 1988: p. Medium: X; Size: Pages: 67-69.
22. Gupta, A. and D. Subba Rao, *Model for the performance of a fluid catalytic cracking (FCC) riser reactor: effect of feed atomization.* Chemical Engineering Science, 2001. **56**(15): p. 4489-4503.
23. Occelli, M.L. and P. O'Connor, *Fluid Catalytic Cracking V*2001: Elsevier Science.
24. Yaws, C.L., *Thermophysical Properties of Chemicals and Hydrocarbons*2014: Elsevier Science.
25. Yaws, C.L., *Transport Properties of Chemicals and Hydrocarbons*2014: Elsevier Science.
26. Yaws, C.L., P.K. Narasimhan, and C. Gabbula, *Yaws' Handbook of Antoine Coefficients for Vapor Pressure (2nd Electronic Edition)*, Knovel.
27. Riazi, R., *Characterization and Properties of Petroleum Fractions*2005: ASTM International.
28. Du, Y., et al., *An integrated methodology for the modeling of Fluid Catalytic Cracking (FCC) riser reactor.* Applied Petrochemical Research, 2014. **4**(4): p. 423-433.
29. Fuller, E.N., P.D. Schettler, and J.C. Giddings, *NEW METHOD FOR PREDICTION OF BINARY GAS-PHASE DIFFUSION COEFFICIENTS.* Industrial & Engineering Chemistry, 1966. **58**(5): p. 18-27.
30. Hirt, C.W. and B.D. Nichols, *Volume of fluid (VOF) method for the dynamics of free boundaries.* Journal of Computational Physics, 1981. **39**(1): p. 201-225.
31. Ubbink, O., *Numerical prediction of two fluid systems with sharp interfaces*, 1997, Imperial College.
32. *FLUENT 14.5.* Theory Guide, 2011.
33. Malgarinos, I., et al., *VOF simulations of the contact angle dynamics during the drop spreading: Standard models and a new wetting force model.* Advances in Colloid and Interface Science, 2014. **212**(0): p. 1-20.
34. Malgarinos, I., N. Nikolopoulos, and M. Gavaises, *A numerical study on droplet-particle collision dynamics.* International Journal of Heat and Fluid Flow.
35. Sazhin, S.S., *Advanced models of fuel droplet heating and evaporation.* Progress in Energy and Combustion Science, 2006. **32**(2): p. 162-214.
36. Kryukov, A.P., V.Y. Levashov, and S.S. Sazhin, *Evaporation of diesel fuel droplets: kinetic versus hydrodynamic models.* International Journal of Heat and Mass Transfer, 2004. **47**(12–13): p. 2541-2549.
37. Nikolopoulos, N., A. Theodorakakos, and G. Bergeles, *A numerical investigation of the evaporation process of a liquid droplet impinging onto a hot substrate.* International Journal of Heat and Mass Transfer, 2007. **50**(1–2): p. 303-319.
38. Hardt, S. and F. Wondra, *Evaporation model for interfacial flows based on a continuum-field representation of the source terms.* J. Comput. Phys., 2008. **227**(11): p. 5871-5895.
39. Strotos, G., et al., *Numerical investigation on the evaporation of droplets depositing on heated surfaces at low Weber numbers.* International Journal of Heat and Mass Transfer, 2008. **51**(7–8): p. 1516-1529.
40. Froment, G.F. and K.B. Bischoff, *Chemical reactor analysis and design*1979: Wiley.
41. Gianetto, A., et al., *Fluid Catalytic Cracking Catalyst for Reformulated Gasolines. Kinetic Modeling.* Industrial & Engineering Chemistry Research, 1994. **33**(12): p. 3053-3062.

42. Bakshi, S., I.V. Roisman, and C. Tropea, *Investigations on the impact of a drop onto a small spherical target.* Physics of Fluids (1994-present), 2007. **19**(3): p. -.
43. Zhang, D., K. Papadikis, and S. Gu, *Application of a high density ratio lattice-Boltzmann model for the droplet impingement on flat and spherical surfaces.* International Journal of Thermal Sciences, 2014. **84**(0): p. 75-85.
44. Wong, S.C. and A.C. Lin, *Internal temperature distributions of droplets vaporizing in high-temperature convective flows.* Journal of Fluid Mechanics, 1992. **237**: p. 671-687.
45. Strotos, G., et al., *Numerical investigation of the evaporation of two-component droplets.* Fuel, 2011. **90**(4): p. 1492-1507.
46. Nomura, H., et al., *Experimental study on high-pressure droplet evaporation using microgravity conditions.* Symposium (International) on Combustion, 1996. **26**(1): p. 1267-1273.
47. Qiao, Y.M. and S. Chandra, *Boiling of droplets on a hot surface in low gravity.* International Journal of Heat and Mass Transfer, 1996. **39**(7): p. 1379-1393.
48. Ge, Y., *3D numerical study on droplet-solid collisions in the Leidenfrost regime*, 2005, The Ohio State University: Ann Arbor. p. 246-246 p.
49. Harvie, D.J.E. and D.F. Fletcher, *A hydrodynamic and thermodynamic simulation of droplet impacts on hot surfaces, Part II: validation and applications.* International Journal of Heat and Mass Transfer, 2001. **44**(14): p. 2643-2659.